Dalton Transactions

PAPER

View Article Online
View Journal | View Issue

Cite this: *Dalton Trans.*, 2014, **43**, 2161

Electronic tuning of nitric oxide release from manganese nitrosyl complexes by visible light irradiation: enhancement of nitric oxide release efficiency by the nitro-substituted quinoline ligand†

Yutaka Hitomi,* Yuji Iwamoto and Masahito Kodera

Received 27th June 2013,
Accepted 8th November 2013

DOI: 10.1039/c3dt51719e

www.rsc.org/dalton

Manganese nitrosyl $\{MnNO\}^6$ complexes of general formula $[Mn(dpaq^R)(NO)]ClO_4$ ($\mathbf{1^R}$), where $dpaq^R$ denotes a series of pentadentate monoamido ligands, 2-[*N*,*N*-bis(pyridin-2-ylmethyl)]-amino-*N*′-quinolin-8-yl-acetamido with R = OMe, H, Cl and NO_2 at the 5-position of the quinoline moiety, were prepared. The derivatives $\mathbf{1^R}$ were characterized by ^{1}H NMR, IR and UV–vis spectrometry as well as by single-crystal X-ray crystallography. The N–O bond and the amido C=O bond stretching frequencies, as well as the redox potentials of $\mathbf{1^R}$ derivatives, substantially varied depending on the nature of the substituent group R on the quinoline ring, indicating that the π back-bonding from Mn to NO groups becomes weak as the substituent group R becomes more electron withdrawing. The nitro-substituted derivative $\mathbf{1^{NO2}}$ is unique among the series; the tail of its absorption bands extends to the NIR region (up to 700 nm), and the apparent NO releasing rate from $\mathbf{1^{NO2}}$ by light irradiation at 650 nm was *ca.* 4-fold higher than the other derivatives.

Introduction

Nitric oxide (NO) is well established as a signaling molecule that functions in the cardiovascular, nervous, and immune systems.[1–3] The biological roles of NO not only explain the action of nitroglycerin, organic nitrates, and sodium nitroprusside, all of which have been used as therapeutic agents for a long time, but also lead to development of various NO-releasing molecules (NORMs), because they are expected to be useful tools for biological research. In addition, NORMs—such as organic nitrites and nitrates, *S*-nitroso compounds, and diazeniumdiolates[4–7] and metal nitrosyl complexes[8]—are expected to be potential therapeutic agents. In the past decade, photoactive NORMs (PhotoNORMs)[9] have received much attention because they can deliver NO to biological targets in a temporally and spatially controlled manner.[10–15] PhotoNORMs are stable in aqueous solutions in the dark and only release NO upon photoirradiation at an appropriate wavelength. To minimize tissue damage caused by photoirradiation, it is desirable to produce PhotoNORMs that can effectively release NO by low-intensity light irradiation at long wavelengths. Metal nitrosyl complexes are promising PhotoNORM candidates since many of these complexes release NO by photo-irradiation. Photosensitizers are often used to construct PhotoNORMs that can be activated by light irradiation at desired wavelengths;[11,13] such dye-sensitized PhotoNORMs include *trans*-$Cr(cyclam)(ONO)_2^+$ complexes having pendant aromatic chromophores (cyclam = 1,4,8,11-tetraazacyclotetradecane),[16] electrostatic assemblies between anionic semiconductor quantum dots and cationic *trans*-$Cr(cyclam)(ONO)_2^+$,[17] dye-attached iron/sulfur/nitrosyl clusters $Fe_2(\mu\text{-}RS)_2(NO)_4$,[18,19] and ruthenium nitrosyl complexes having NIR dyes as ligands.[20,21] Appropriate ligand designs for metal nitrosyls are a powerful alternative approach.[22,23] For example, Mascharak's group reported that a diamagnetic manganese nitrosyl complex represented as $\{MnNO\}^6$ in the Enemark–Feltham notation,[24] $[Mn(PaPy_3)(NO)]ClO_4$ ($PaPy_3$ = *N*,*N*-bis(2-pyridylmethyl)amine-*N*-ethyl-2-pyridine-2-carboxamido), has an absorption band at around 650 nm and releases NO in aqueous media when exposed to visible light of low intensity (ϕ = 0.55 and λ_{irr} = 532 nm).[25,26] Recent theoretical studies have provided insight into the transitions that lead to NO release by photo-irradiation.[27–29] Notably, $[Mn(PaPy_3)(NO)]ClO_4$ has been successfully applied for activating soluble guanylate cyclase or for eradicating bacteria.[30–33] More importantly, the sensitivity of the $\{MnNO\}^6$ complex against low-energy light can be further enhanced by replacing a pyridine

Department of Molecular Chemistry and Biochemistry, Faculty of Science and Engineering, Doshisha University, 1–3 Tatara Miyakodani, Kyotanabe, Kyoto 610–0321, Japan. E-mail: yhitomi@doshisha.ac.jp

†Electronic supplementary information (ESI) available: Crystallographic data, and additional tables and figures. CCDC 947309–947312. For ESI and crystallographic data in CIF or other electronic format see DOI: 10.1039/c3dt51719e

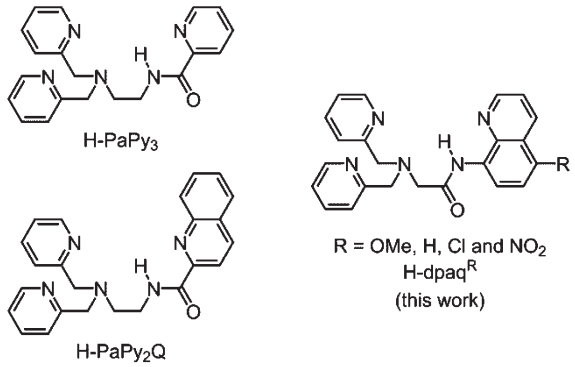

Chart 1 Chemical structures of supporting ligands.

with a quinoline ring.[23] We focused on the latter ligand design approach owing to its simplicity and ability to synthesize relatively small PhotoNORMs compared to dye-sensitized PhotoNORMs.

In this study, we aimed to clarify how the supporting ligand of $\{MnNO\}^6$ complexes changes the electronic structures and consequently the NO release efficiency upon photo-irradiation. Herein, we have used a series of pentadentate monoamido ligands, where $dpaq^R$ denotes four pentadentate monoamido ligands, 2-[*N*,*N*-bis(pyridin-2-ylmethyl)]-amino-*N*′-quinolin-8-yl-acetamido with R = OMe, H, Cl and NO_2 at the 5-position of the quinoline moiety (Chart 1), which we recently prepared in our laboratory,[34,35] to construct a series of $\{MnNO\}^6$ complexes. We expected that the substituted group on the quinoline ligand should modulate the coordination strength of the amido ligand, and that the stronger amido coordination should donate more electron density to the Mn center, increasing the π back-bonding from the Mn to the NO ligand. Herein, we present the syntheses and structures of a series of $\{MnNO\}^6$ complexes, $[Mn(dpaq^R)(NO)]ClO_4$ (**1**^{R}, R = OMe, H, Cl and NO_2), and their NO-release efficiency upon photoirradiation at specific wavelengths.

Results and discussion

Syntheses

Mn(II) complexes $[Mn(II)(dpaq^R)]ClO_4$ were synthesized by reacting $Mn(ClO_4)_2$ with H-$dpaq^R$ ligand in the presence of Et_3N in CH_3CN, obtained as white solids and found to be air stable in the solid state. Respective nitrosyl complexes **1**^{R} were synthesized by bubbling purified NO gas in the $[Mn(II)(dpaq^R)]ClO_4$ solution in CH_3CN under anaerobic conditions. In most cases, the colour of the reaction mixture changed from yellow to brown within 30 s during NO bubbling. All nitrosyl complexes **1**^{R} were obtained as brown solids that were air stable in the dark. All **1**^{R} complexes were soluble in CH_3CN and H_2O; however, they were not soluble in less polar solvents, such as hexane or CH_2Cl_2.

Crystallography

Crystals of **1**^{R} suitable for X-ray diffraction were reproducibly grown by vapour diffusion of ethyl acetate into the CH_3CN solution of **1**^{R} derivatives at room temperature (Fig. 1). The coordination structures of **1**^{R} derivatives resemble the reported structure of $[Mn(PaPy_3)(NO)]ClO_4$ (**2**)[26] and $[Mn(PaPy_2Q)(NO)]ClO_4$ (**3**),[23] *i.e.*, the metal centres are in a distorted octahedral geometry, and the amido nitrogen is located *trans* to NO. The Mn–N–O angles are nearly linear as observed for $\{MnNO\}^6$ complexes.[23,26,36–38] The N–O and Mn–NO bonds range from 1.02 to 1.14 Å and from 1.63 to 1.74 Å, respectively, which is comparable to those observed for **2** and **3** (Table 1).[23,26] However, the metric parameters of the $\{MnNO\}^6$ unit in **1**^{R} compounds do not show a clear correlation that is expected by the substituted groups on the ligand, which may be caused by the disorder of the NO ligand. On the other hand, the Mn–N_4 (amido) bond distance increases, and the C=O bond distance gradually decreases as the substituent becomes more electron withdrawing (Table 1), showing that the substitution groups modulate the coordination strength of the amido ligand as expected.

NMR spectra

^{1}H NMR spectra of **1**^{R} were measured in CD_3CN, and all signals appear in the range of 4.0–9.4 ppm (Fig. S1†), as observed for the diamagnetic $\{MnNO\}^6$ complexes **2** and **3**.[23,26] Peak assignments are listed in Table S3.† A singlet at *ca.* 4 ppm was attributed to the CH_2 moiety next to the carboxamido ligand. An AB quartet at *ca.* 4.4 and *ca.* 4.6 ppm (J_{AB} = 15.5 Hz) was ascribed to CH_2 moieties of two pyridylmethyl arms. These ^{1}H NMR signals are in agreement with the C_s symmetry, suggesting that the crystal structure is retained in the

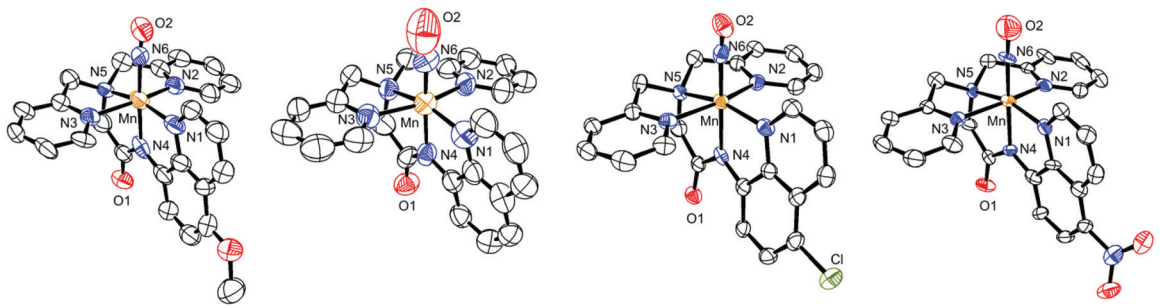

Fig. 1 Ortep representation of the cation of **1**^{R} derivatives at 50% probability level. H atoms are omitted for clarity.

Table 1 Selected angle, bond lengths, and stretching frequencies of $\{MnNO\}^6$ complexes

	Mn–N–O/°	N–O/Å	Mn–NO/Å	Mn–N_{amido}/Å	C═O/Å	ν_{NO}/cm^{-1}	ν_{CO}/cm^{-1}
$\mathbf{1^{OMe}}$	176.7(8)	1.015(7)	1.742(8)	1.923(7)	1.247(9)	1737	1602
$\mathbf{1^{H}}$	171(2)	1.022(16)	1.635(12)	1.998(9)	1.225(15)	1739	1612
$\mathbf{1^{Cl}}$	171.3(3)	1.044(4)	1.713(4)	1.941(3)	1.240(4)	1743	1624
$\mathbf{1^{NO2}}$	175.8(6)	1.136(7)	1.660(5)	1.957(5)	1.217(7)	1744	1636
2[a]	171.91(13)	1.1918(18)	1.6601(14)	1.9551(14)	1.244(2)	1745	1627
3[b]	171.5(8)	1.237(18)	1.678(3)	1.956(3)	1.243(4)	1725	1634

[a] Data from ref. 26. [b] Data from ref. 23.

solution. ^{1}H NMR spectra of all the $\mathbf{1^R}$ derivatives were nearly identical, except for protons at 4- and 6-positions of the quinoline ring. The proton signals shifted by +0.88 and +0.95 ppm from R = H to R = NO_2; the shifts of the other signals were within 0.10 ppm (Table S3†).

IR spectra

In the solid state IR spectra of $\mathbf{1^R}$ compounds, two intense vibration bands were observed (Fig. S2†). One signal appeared in the range of 1737–1744 cm^{-1}, while the other signal was found in the range of 1602–1636 cm^{-1} (Table 1). The band at a higher wavenumber arises from the N–O vibration, while the band at a lower wavenumber corresponds to the C═O stretching vibration of the carboxamido moiety. The N–O vibration values are similar to the N–O stretch for **2** and **3**. Both C═O and N–O bands shifted to a higher energy as the substituent became electron withdrawing. The observed changes for the C═O vibration are consistent with those for the C═O bond distance in their crystal structures. The changes for C═O and N–O bands show a clear linear correlation (Fig. 2). These results suggest that, as the substituent group became more electron withdrawing, the strength of carboxamido ligation decreased together with the π back-bonding from the Mn to NO ligand.

Electrochemistry

Compounds $\mathbf{1^R}$ exhibited a quasi-reversible $\{MnNO\}^5/\{MnNO\}^6$ couple in the range of 0.49–0.63 V *versus* Fc^+/Fc in CH_3CN (Fig. S3†). The redox potential of **2** was 0.50 V *versus* Fc^+/Fc, indicating that $dpaq^R$ ligands with R = NO_2, Cl and H are weaker donor ligands than $PaPy_3$. The stability of the $\{MnNO\}^6$ state decreases in the order of R = NO_2 > Cl > H > OMe. The redox potentials follow a linear relationship against the Hammett substituent constants with ρ-values of 131 ± 6 (Fig. 3), which clearly illustrates the substituent effect on the $\{MnNO\}^6$ unit.

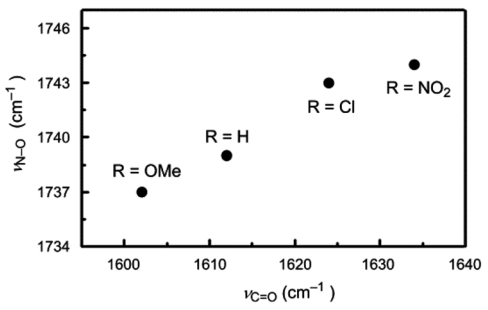

Fig. 2 Correlation graph of ν_{N-O} and $\nu_{C=O}$ frequencies for $\mathbf{1^R}$ derivatives.

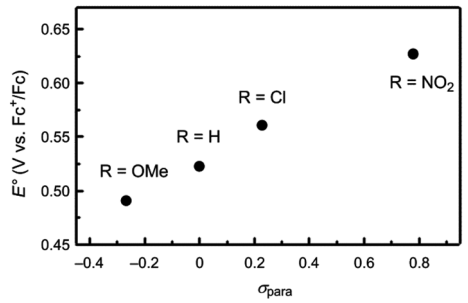

Fig. 3 Hammett plot for the redox potential of $\mathbf{1^R}$ derivatives.

Absorption spectra

The solutions of ligands H-$dpaq^R$ and their Mn(II) complexes [Mn(II)$dpaq^R$]ClO_4 in CH_3CN show two absorption bands at around 250 and 350 nm (Fig. 4 and Table S5†). These bands should be assignable to π–π* transitions of quinoline rings. The bands of [Mn(II)$dpaq^R$]ClO_4 appear at a lower energy than those of the respective ligands, owing to the metalation of the carboxamide moiety of H-$dpaq^R$. The energy of the bands at around 350 nm decreases in the order of R = H > Cl > OMe > NO_2 in both series of H-$dpaq^R$ and [Mn(II)$dpaq^R$]ClO_4. Especially, large bathochromic shifts were observed for nitro-substituent derivatives, H-$dpaq^{NO2}$ and [Mn(II)$dpaq^{NO2}$]ClO_4, which should be caused by stabilization of quinoline π* orbitals because of the nitro group.

While the solutions of [Mn(II)$dpaq^R$]ClO_4 in CH_3CN are colourless for R = H and Cl, pale yellow for R = OMe and yellow for R = NO_2, nitrosyl complexes $\mathbf{1^R}$ in CH_3CN are yellow. The absorption spectra of $\mathbf{1^{OMe}}$, $\mathbf{1^{H}}$ and $\mathbf{1^{Cl}}$ in CH_3CN have similar features, showing two absorption bands ranging from 357 to 475 nm and a very weak broad band at around 600 nm (Fig. 5). On the other hand, $\mathbf{1^{NO2}}$ showed an intense band at 423 nm, a weak band at 513 nm and a weak shoulder band at 650 nm (ε = 493 M^{-1} cm^{-1}). Thus, the tail of absorption bands of $\mathbf{1^{NO2}}$ extends to the NIR region (up to 700 nm), which should correlate to the bathochromic shifts observed for H-$dpaq^{NO2}$ and [Mn(II)$dpaq^{NO2}$]ClO_4. The absorption spectra of $\mathbf{1^R}$ derivatives

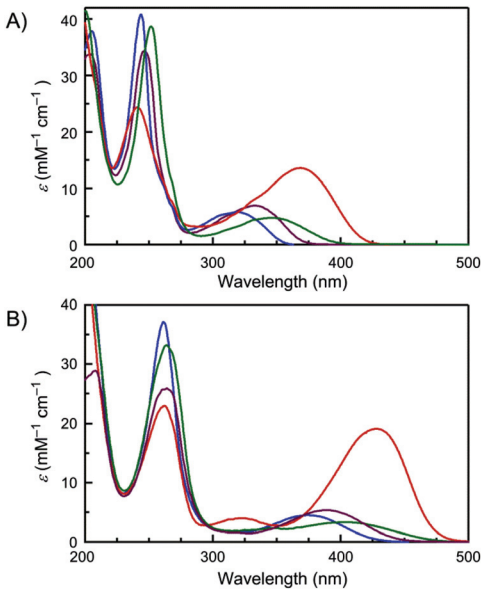

Fig. 4 Electric absorption spectra of H-dpaq^{R} (A) and [Mn(dpaq^{R})]ClO$_4$ (B) in CH_3CN at 20 °C. R: OMe, green; H, blue; Cl, purple and NO_2, red.

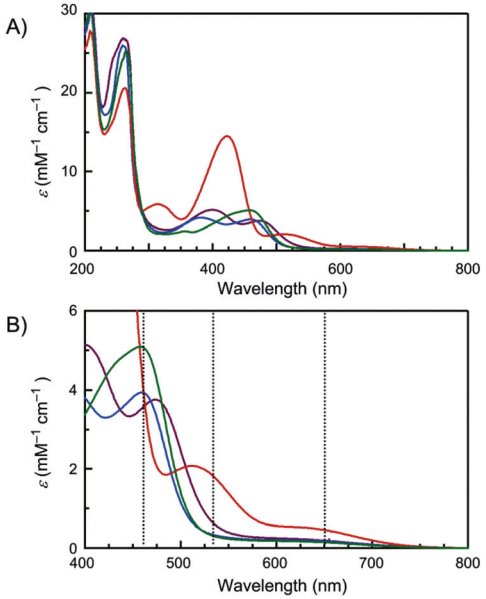

Fig. 5 Electric absorption spectra of $\mathbf{1}^{R}$ (A) in CH_3CN at 20 °C. R: OMe, green; H, blue; Cl, purple and NO_2, red. Panel B shows a magnification in the range of 400 to 800 nm. Vertical dotted lines show the wavelengths of light irradiation (460, 530 and 650 nm).

in MES buffer (pH 7.2) were almost identical to those in MeCN (Fig. S4 and Table S5†).

Photoinduced NO release

The nitrosyl complexes $\mathbf{1}^{R}$ are stable in aqueous media even at 37 °C in the dark over 10 days. Under UV light irradiation, however, these complexes rapidly transformed into the corresponding Mn(II) complexes. Formation of NO concomitant with

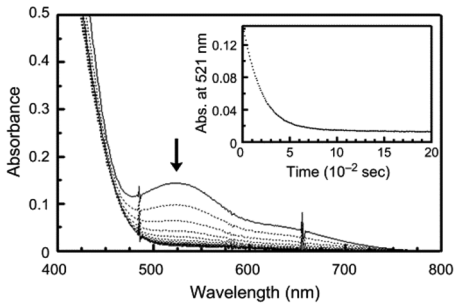

Fig. 6 Electronic spectral change of a solution of $\mathbf{1}^{NO2}$ in MES buffer (pH 7.2, 5% DMSO) at 20 °C under irradiation at 650 nm. The arrow indicates a decrease in band intensities as the reaction proceeds. Inset: time profile of the absorbance at 521 nm.

the decomposition of $\mathbf{1}^{R}$ was verified by assay using reduced myoglobin (Fig. S5†). We further investigated the dependence of the conversion rate on irradiation wavelength. The conversion of $\mathbf{1}^{R}$, together with **2** as a reference, was spectrophotometrically monitored in MES buffer (pH 7.2, 5% DMSO) at 20 °C under irradiation at 460, 530 and 650 nm. The light at the wavelength was kept at the same intensity (300 mW m^{-2}). The absorption bands characteristic to $\mathbf{1}^{R}$ and **2** (457 nm for $\mathbf{1}^{OMe}$, 461 nm for $\mathbf{1}^{H}$, 475 nm for $\mathbf{1}^{Cl}$, 521 nm for $\mathbf{1}^{NO2}$ and 450 nm for **2**) disappeared within 30 min under light irradiation (Fig. 6 and S5†). The decay rates were dependent on the irradiation wavelength; the decomposition of $\mathbf{1}^{R}$ became slower in the order of $\mathbf{1}^{OMe} \approx \mathbf{1}^{H} > \mathbf{1}^{Cl} > \mathbf{1}^{NO2}$ under light irradiation at 460 nm, while the order was reversed in the case of irradiation at 530 or 650 nm, $\mathbf{1}^{OMe} < \mathbf{1}^{H} < \mathbf{1}^{Cl} < \mathbf{1}^{NO2}$. Notably, the decay of $\mathbf{1}^{NO2}$ by light irradiation at 650 nm was *ca.* 4-fold faster than the other derivatives.

The quantum yields (QYs) of NO release from $\mathbf{1}^{R}$ upon light irradiation at 460 nm were almost indistinguishable, falling between 0.58 and 0.66 (Table 2). Although the QYs at 530 and 650 nm for $\mathbf{1}^{Cl}$ and $\mathbf{1}^{NO2}$ were slightly higher than those for $\mathbf{1}^{OMe}$ and $\mathbf{1}^{H}$, the small difference in the QYs cannot account for the observed 4-fold faster NO-release from $\mathbf{1}^{NO2}$ under light irradiation at 650 nm. The similar QYs for $\mathbf{1}^{R}$ series indicate that there is no significant difference in the inherent reactivity of the excited states formed from $\mathbf{1}^{R}$ derivatives. The faster NO release from $\mathbf{1}^{NO2}$ under light irradiation at 650 nm should be mainly attributed to the higher absorption coefficients of $\mathbf{1}^{NO2}$ at 650 nm (Table 2), because the rate of a photochemical process is proportional to the intensity of the light absorbed and to the quantum yield.[39]

Conclusions

Depending on the electronic nature of the substituent group of the quinoline ring, the NO vibration frequencies of $\mathbf{1}^{R}$ and the redox potentials of $\{MnNO\}^5/\{MnNO\}^6$ couple vary substantially. For example, compound $\mathbf{1}^{NO2}$ shows the highest NO frequency and redox potential, suggesting weak π back-bonding

Table 2 Molar extinction coefficients and quantum yields for NO release at specific wavelengths

	ε (mM^{-1} cm^{-1})			ϕ (mol $einstein^{-1}$)		
Complex	460 nm	530 nm	650 nm	460 nm	530 nm	650 nm
$\mathbf{1}^{OMe}$	4.20	0.370	0.111	0.58 ± 0.04	0.47 ± 0.01	0.49 ± 0.01
$\mathbf{1}^{H}$	3.11	0.363	0.123	0.61 ± 0.03	0.51 ± 0.01	0.47 ± 0.01
$\mathbf{1}^{Cl}$	2.69	0.707	0.113	0.66 ± 0.04	0.66 ± 0.02	0.73 ± 0.01
$\mathbf{1}^{NO2}$	1.77	1.56	0.493	0.61 ± 0.05	0.63 ± 0.01	0.78 ± 0.01
2	2.04	0.113	0.220	0.71 ± 0.04	0.59 ± 0.02	0.39 ± 0.01

from the Mn to the NO ligand in $\mathbf{1}^{NO2}$. Therefore, we first expected that $\mathbf{1}^{NO2}$ should be the most active PhotoNORM among $\mathbf{1}^{R}$. However, the reactivity order of NO release from $\mathbf{1}^{R}$ was highly dependent on the irradiation wavelength, but was independent of the electronic nature of the substituent groups. Thus, the rates of photoinduced NO release from $\mathbf{1}^{R}$ are exclusively determined by the absorption coefficient, at which wavelength light is absorbed.

The nitro-substituted derivative $\mathbf{1}^{NO2}$ exhibited absorption bands extending up to 700 nm, which should be caused by the stabilization of the quinoline π* orbital by introduction of the nitro group on the quinoline ring. Because of this absorption band, $\mathbf{1}^{NO2}$ can release NO by photo-irradiation at 650 nm with a *ca.* 4-fold higher rate than the other derivatives. Our results suggest that the stabilization of π* orbitals of the aromatic ligand to Mn is a promising strategy to design {MnNO}^{6} PhotoNORMs that can release NO with even higher efficiency by light irradiation at long wavelengths.

Experimental section

General

The reagents and the solvents used in this study, except the ligands and the manganese complexes, were commercial products of the highest available purity and were further purified by standard methods, if necessary. Ligand H-dpaq^{H} was prepared according to the reported procedure.[34] The other ligands H-dpaq^{R} (R = OMe, Cl and NO_2) were synthesized through procedures similar to that for H-dpaq^{H}. Details will be reported elsewhere.[35] [Mn($PaPy_3$)(NO)]ClO_4 (**2**) was prepared following the procedure reported by Ghosh *et al.*[26] Room temperature ^{1}H NMR spectra were recorded using a JMN-A 500 spectrometer at 500 MHz frequency. Infrared spectra (IR) were recorded on a Shimadzu IRAffinity-1 spectrometer with a Pike MIRacle10 ATR system (ZnSe). Electrospray ionization mass spectroscopy was performed on a JEOL JMS-T100CS spectrometer. Electronic spectra of complexes were recorded using an Agilent 8543 UV–vis spectrometer. Cyclic voltammograms were recorded by a Bioanalytical Systems (BAS) model CV-50W instrument using dry and degassed CH_3CN solutions with 0.1 M NBu_4ClO_4 and 1 mM complexes. The electrodes were as follows: Pt (working), Pt wire (auxiliary), and Ag/AgCl in CH_3CN (reference). At the end of each measurement, the potentials were internally calibrated using Fc^+/Fc couple, and presented with respect to the Fc^+/Fc couple at the same scan rate (20 mV s^{-1}).

Synthesis of the manganese(II) complexes

Caution! *Perchlorate salts of metal complexes are potentially explosive. Only small quantities of the material should be prepared, and the samples should be handled with care.*

A solution of H-dpaq^{R} (0.26 mmol) in CH_3CN (2 mL) containing Et_3N (40 μL, 0.29 mmol) was added to a solution of Mn-$(ClO_4)_2$·$6H_2O$ (0.11 g, 0.31 mmol) in CH_3CN (0.5 mL) at room temperature. The mixture was stirred for 2 h. The precipitate was collected, washed with diethyl ether, and dried *in vacuo*.

[Mn(dpaq^{OMe})]ClO_4. Yellow solid. Yield: 55%. Anal. calcd for [Mn(dpaq^{OMe})]$(ClO_4)(H_2O)_{0.5}$: C, 50.06; H, 4.03; N, 12.16. Found: C, 50.22; H, 4.00; N, 12.35. Selected IR frequencies (cm^{-1}, FT-ATR): 1549 (CO). Electronic absorption spectrum in CH_3CN (nm (M^{-1} cm^{-1})): 405 (3320), 346 (2330), 264 (33 200). Electronic absorption spectrum in MES buffer (pH 7.2, 5% DMSO) (nm (M^{-1} cm^{-1})): 334 (4270), 248 (29 200). ESI-MS, positive mode: *m*/*z* 467.19 {Mn(dpaq^{OMe})}$^+$.

[Mn(dpaq^{H})]ClO_4. Pale yellow solid. Yield: 90%. Anal. calcd for [Mn(dpaq^{H})]$(ClO_4)(H_2O)_{0.8}$: C, 50.11; H, 3.95; N, 12.70. Found: C, 50.19; H, 3.81; N, 12.74. Selected IR frequencies (cm^{-1}, FT-ATR): 1541 (CO). Electronic absorption spectrum in CH_3CN (nm (M^{-1} cm^{-1})): 375 (4500), 262 (37 100). Electronic absorption spectrum in MES buffer (pH 7.2, 5% DMSO) (nm (M^{-1} cm^{-1})): 309 (5300), 241 (23 800). ESI-MS, positive mode: *m*/*z* 437.08 {Mn(dpaq^{H})}$^+$.

[Mn(dpaq^{Cl})]ClO_4. Pale yellow solid. Yield: 84%. Anal. calcd for [Mn(dpaq^{Cl})]$(ClO_4)(H_2O)_{0.5}$: C, 47.61; H, 12.07; N, 3.47. Found: C, 47.76; H, 11.89; N, 3.48. Selected IR frequencies (cm^{-1}, FT-ATR): 1537 (CO). Electronic absorption spectrum in CH_3CN (nm (M^{-1} cm^{-1})): 388 (5330), 264 (25 900). Electronic absorption spectrum in MES buffer (pH 7.2, 5% DMSO) (nm (M^{-1} cm^{-1})): 325 (5280), 244 (25 300). ESI-MS, positive mode: *m*/*z* 471.12 {Mn(dpaq^{Cl})}$^+$.

[Mn(dpaq^{NO2})]ClO_4. Orange solid. Yield: 93%. Anal. calcd for [Mn(dpaq^{NO2})]$(ClO_4)(H_2O)_{0.5}$: C, 46.76; H, 3.41; N, 14.22. Found: C, 47.03; H, 3.26; N, 13.92. Selected IR frequencies (cm^{-1}, FT-ATR): 1533 (CO). Electronic absorption spectrum in CH_3CN (nm (M^{-1} cm^{-1})): 428 (19 100), 322 (3990), 262 (22 900). Electronic absorption spectrum in MES buffer (pH 7.2, 5% DMSO) (nm (M^{-1} cm^{-1})): 380 (10 100), 238 (12 000). ESI-MS, positive mode: *m*/*z* 482.15 {Mn(dpaq^{NO2})}$^+$.

Synthesis of {MnNO}^{6} complexes

All procedures were performed in the dark. A solution of [Mn(dpaq^R)]ClO_4 (0.093 mmol) in CH_3CN (1.5 mL)] was degassed and bubbled with purified NO gas (50 mL × 3) with vigorous stirring. Brown precipitates were filtered, washed with Et_2O, and dried under vacuum.

[Mn(dpaq^{OMe})(NO)]ClO_4. Dark green solid. Yield: 65%. Anal. calcd for [Mn(NO)(dpaq^{OMe})]$(ClO_4)(CH_3CN)_{0.5}$: C, 48.64; H, 3.84; N, 14.75. Found: C, 48.79; H, 3.84; N, 14.75. ^{1}H NMR (500 MHz, CD_3CN): 9.27 (dd, 1H), 8.90 (d, 1H), 8.63 (dd, 1H), 7.82 (t, 2H), 7.63 (dd, 1H), 7.47 (d, 2H), 7.15 (d, 1H), 7.02 (t, 2H), 6.33 (d, 2H), 4.55 (d, 2H), 4.35 (d, 2H), 4.03 (s, 3H), 3.95 (s, 2H). Selected IR frequencies (cm^{-1}, FT-ATR): 1737 (NO), 1602 (CO). Electronic absorption spectrum in CH_3CN (nm (M^{-1} cm^{-1})): 459 (5090), 356 (2450), 265 (25 300). Electronic absorption spectrum in MES buffer (pH 7.2) (nm (M^{-1} cm^{-1})): 457 (4230), 398 (3830).

[Mn(dpaq^H)(NO)]ClO_4. Brown solid. Yield: 75%. Anal. calcd for [Mn(NO)(dpaq^H)]$(ClO_4)(H_2O)$: C, 47.23; H, 3.79; N, 14.37. Found: C, 47.18; H, 3.55; N, 14.23. ^{1}H NMR (500 MHz, CD_3CN): 9.25 (d, 1H), 8.97 (d, 1H), 8.39 (d, 1H), 7.83 (t, 2H), 7.72 (t, 1H), 7.65 (dd, 1H), 7.63 (d, 1H), 7.48 (d, 2H), 7.02 (t, 2H), 6.31 (d, 2H), 4.57 (d, 2H), 4.37 (d, 2H), 4.00 (s, 2H). Selected IR frequencies (cm^{-1}, FT-ATR): 1739 (NO), 1612 (CO). Electronic absorption spectrum in CH_3CN (nm (M^{-1} cm^{-1})): 459 (3940), 382 (4160), 259 (25 900). Electronic absorption spectrum in MES buffer (pH 7.2) (nm (M^{-1} cm^{-1})): 461 (3120), 357 (3910).

[Mn(dpaq^{Cl})(NO)]ClO_4. Brown solid. Yield: 60%. Anal. calcd for [Mn(NO)(dpaq^{Cl})]$(ClO_4)(H_2O)_{0.75}$: C, 45.25; H, 3.10; N, 13.31. Found: C, 44.93; H, 3.36; N, 13.67. ^{1}H NMR (500 MHz, CD_3CN): 9.33 (d, 1H), 8.92 (d, 1H), 8.63 (d, 1H), 7.84 (t, 2H), 7.77 (m, 2H), 7.48 (d, 2H), 7.03 (t, 2H), 6.35 (d, 2H), 4.56 (d, 2H), 4.36 (d, 2H), 3.99 (s, 2H). Selected IR frequencies (cm^{-1}, FT-ATR): 1743 (NO), 1624 (CO). Electronic absorption spectrum in CH_3CN (nm (M^{-1} cm^{-1})): 474 (3760), 398 (5140), 260 (26 900). Electronic absorption spectrum in MES buffer (pH 7.2) (nm (M^{-1} cm^{-1})): 475 (2960), 375 (4560).

[Mn(dpaq^{NO2})(NO)]ClO_4. Dark drown solid. Yield: 75%. Anal. calcd for [Mn(NO)(dpaq^{NO2})](ClO_4)(diethyl ether)$_{0.25}$: C, 45.73; H, 3.44; N, 15.55. Found: C, 45.60; H, 3.35; N, 15.64. ^{1}H NMR (500 MHz, CD_3CN): 9.39 (d, 1H), 9.27 (d, 1H), 8.96 (d, 1H), 8.67 (d, 1H), 7.85 (m, 3H), 7.46 (d, 2H), 7.05 (t, 2H), 6.41 (d, 2H), 4.59 (d, 2H), 4.38 (d, 2H), 4.05 (s, 2H). Selected IR frequencies (cm^{-1}, FT-ATR): 1744 (NO), 1636 (CO). Electronic absorption spectrum in CH_3CN (nm (M^{-1} cm^{-1})): 513 (2070), 423 (14 500), 314 (5870), 264 (20 600). Electronic absorption spectrum in MES buffer (pH 7.2) (nm (M^{-1} cm^{-1})): 523 (1570), 392 (10 300).

X-ray crystallography

Brown crystals of manganese nitrosyl complexes were obtained by vapour diffusion of acetonitrile into the ethyl acetate solution of the complex. X-ray quality single crystals were mounted on tips made from polymer films (MicroMount). The intensities were recorded on a Rigaku R-AXIS RAPID IP X-ray diffractometer using graphite-monochromatized Cu-Kα radiation (λ = 1.54187 Å), operating at 133 K. The structures have been solved by direct methods using SIR2004[40] and were refined using the Shelx-97 program package.[41] The hydrogen atoms residing in the carbon atoms were located geometrically. The oxygen atoms of perchlorate anion were judged to be disordered over two sites with 50% population each for **1^{OMe}**, and over three sites (30 : 30 : 40) for **1^{Cl}**. The perchlorate within **1^H** was judged located at two sites and each perchlorate ion has an occupation factor of 0.5. In the refinement, the Cl–O distances were restrained to 1.42(2) Å. The O···O distances within each perchlorate ion were restrained to be equal and to have same isotropic displacement parameter. Owing to the two-site disorder of the perchlorate anion within **1^H**, the NO moiety of **1^H** showed a large disorder, resulting in the larger *R*-value. All non-hydrogen atoms were refined anisotropically. Important crystallographic parameters and selected bond distances/angles are listed in Tables S1 and S2.†

Kinetic measurements

For kinetic analysis of the decomposition of **1^R** and **2** as a reference in MES buffer (pH 7.2, 5% DMSO) at 20 °C, the decrease in absorbance at 457 nm for **1^{OMe}**, 461 nm for **1^H**, 475 nm for **1^{Cl}**, 521 nm for **1^{NO2}** and 450 nm for **2**, which are characteristic of {MnNO}^{6} species, was monitored as a function of time under irradiation. Solutions of **1^R** or **2** were irradiated from the top of the cell using a 300 W xenon lamp (Asahi Spectra Co. Ltd) through band-pass filters transmitting λ = 460 nm (FWHW: 5 nm), 530 nm (FWHW: 5 nm), and 650 nm (FWHW: 6 nm). The intensity was adjusted at 300 mW m^{-2} measured by photoradiometer HD 2303.0 equipped with an irradiance measurement probe LP471RAD (Delta OHM, S.r.L). The rate constants were obtained from nonlinear least-squares fits of the experimental data to an exponential function.

Quantum yield measurement

Chemical actinometry was used to obtain the photon flux *via* photolysis of Reinecke salt, K[Cr(NH$_3$)$_2$(NCS)$_4$], solutions.[42] The solutions (3 mL) of Reinecke salt in H_2O or {MnNO}^{6} complexes **1^R** and **2** in MES buffer (pH 7.2, 5% DMSO) in a 1 cm quartz cuvette were irradiated from the top of the cell using a 300 W xenon lamp (Asahi Spectra Co. Ltd) through a band-pass filter transmitting λ = 460 nm (FWHW: 5 nm). The intensity was adjusted at 3.1 mW m^{-2}. UV–vis spectra of **1^R** and **2** in MES buffer (pH 7.2, 5% DMSO) were taken after irradiation for 5000 s, and the decomposed fraction was calculated using changes in the absorption spectrum at 457 nm for **1^{OMe}**, 461 nm for **1^H**, 475 nm for **1^{Cl}**, 521 nm for **1^{NO2}** and 450 nm for **2**: 0.146 μmol for **1^{OMe}**, 0.157 μmol for **1^H**, 0.169 μmol for **1^{Cl}**, 0.156 μmol for **1^{NO2}** and 0.182 μmol for **2**, which correspond to less than 10% of the initial complexes. Then, the QYs of **1^R** derivatives were estimated from the decomposition fraction of Reinecke salt (0.0792 μmol) under identical conditions using the reported Reinecke salt's quantum yield with

ϕ = 0.31.[42] The QYs at 530 and 650 nm were estimated based on the QYs at 460 nm and the initial reaction rate constants measured for $\mathbf{1^R}$ derivatives under light irradiation at 460 nm using the following equation: $QY = QY_{460\ nm} \times (k_{int\_460\ nm}/k_{int}) \times (I_{abs}/I_{abs\_460\ nm})$, where k_{int} and I_{abs} denote the initial reaction rate constant and the absorbed light intensity, respectively (Table S6†).

Acknowledgements

We are grateful to the late Suemoto Naoya for his preliminary contribution to this study. We thank Dr Shuhei Furukawa for the kind use of his NOx analyzer and acknowledge useful discussion with Dr Shuhei Furukawa and Dr Stéphane Diring. This work was supported by Grant-in-Aids for Scientific Research (No. 24550197 and 21350037) from the Ministry of Education, Science, Sports, and Culture of Japan.

Notes and references

1 L. J. Ignarro, *Nitric Oxide: Biology and Pathobiology*, Academic Press, San Diego, 2000.
2 S. Kalsner, *Nitric Oxide Free Radicals in Peripheral Neurotransmission*, Birkhauser, Boston, 2000.
3 G. Y. Ko and F. C. Fang, *Nitric Oxide and Infection*, Kluwer Academic/Plenum Publishers, New York, 1999.
4 P. G. Wang, M. Xian, X. Tang, X. Wu, Z. Wen, T. Cai and A. J. Janczuk, *Chem. Rev.*, 2002, **102**, 1091–1134.
5 J. A. Hrabie and L. K. Keefer, *Chem. Rev.*, 2002, **102**, 1135–1154.
6 G. R. Thatcher, *Curr. Top. Med. Chem.*, 2005, **5**, 597–601.
7 H. H. Al-Sa'doni and A. Ferro, *Curr. Med. Chem.*, 2004, **11**, 2679–2690.
8 A. R. Butler and I. L. Megson, *Chem. Rev.*, 2002, **102**, 1155–1166.
9 A. Ostrowski, *Abstracts of Papers, 244th ACS National Meeting & Exposition, Philadelphia, PA, United States, August 19–23, 2012*, 2012, IAC-14.
10 A. D. Ostrowski and P. C. Ford, *Dalton Trans.*, 2009, 10660–10669.
11 P. C. Ford, *Acc. Chem. Res.*, 2008, **41**, 190–200.
12 M. J. Rose and P. K. Mascharak, *Curr. Opin. Chem. Biol.*, 2008, **12**, 238–244.
13 N. L. Fry and P. K. Mascharak, *Acc. Chem. Res.*, 2011, **44**, 289–298.
14 M. J. Rose and P. K. Mascharak, *Coord. Chem. Rev.*, 2008, **252**, 2093–2114.
15 E. Tfouni, M. Krieger, B. R. McGarvey and D. W. Franco, *Coord. Chem. Rev.*, 2003, **236**, 57–69.
16 F. Derosa, X. Bu and P. C. Ford, *Inorg. Chem.*, 2005, **44**, 4157–4165.
17 D. Neuman, A. D. Ostrowski, R. O. Absalonson, G. F. Strouse and P. C. Ford, *J. Am. Chem. Soc.*, 2007, **129**, 4146–4147.
18 S. R. Wecksler, A. Mikhailovsky, D. Korystov, F. Buller, R. Kannan, L. S. Tan and P. C. Ford, *Inorg. Chem.*, 2007, **46**, 395–402.
19 S. R. Wecksler, A. Mikhailovsky, D. Korystov and P. C. Ford, *J. Am. Chem. Soc.*, 2006, **128**, 3831–3837.
20 M. J. Rose and P. K. Mascharak, *Inorg. Chem.*, 2009, **48**, 6904–6917.
21 M. J. Rose, N. L. Fry, R. Marlow, L. Hinck and P. K. Mascharak, *J. Am. Chem. Soc.*, 2008, **130**, 8834–8846.
22 C. G. Hoffman-Luca, A. A. Eroy-Reveles, J. Alvarenga and P. K. Mascharak, *Inorg. Chem.*, 2009, **48**, 9104–9111.
23 A. A. Eroy-Reveles, Y. Leung, C. M. Beavers, M. M. Olmstead and P. K. Mascharak, *J. Am. Chem. Soc.*, 2008, **130**, 4447–4458.
24 J. H. Enemark and R. D. Feltham, *Coord. Chem. Rev.*, 1974, 13.
25 A. A. Eroy-Reveles, Y. Leung and P. K. Mascharak, *J. Am. Chem. Soc.*, 2006, **128**, 7166–7167.
26 K. Ghosh, A. A. Eroy-Reveles, B. Avila, T. R. Holman, M. M. Olmstead and P. K. Mascharak, *Inorg. Chem.*, 2004, **43**, 2988–2997.
27 W. Zheng, S. Wu, S. Zhao, Y. Geng, J. Jin, Z. Su and Q. Fu, *Inorg. Chem.*, 2012, **51**, 3972–3980.
28 N. L. Fry and P. K. Mascharak, *Dalton Trans.*, 2012, **41**, 4726–4735.
29 A. C. Merkle, N. L. Fry, P. K. Mascharak and N. Lehnert, *Inorg. Chem.*, 2011, **50**, 12192–12203.
30 B. J. Heilman, J. St John, S. R. Oliver and P. K. Mascharak, *J. Am. Chem. Soc.*, 2012, **134**, 11573–11582.
31 B. J. Heilman, G. M. Halpenny and P. K. Mascharak, *J. Biomed. Mater. Res. B Appl. Biomater.*, 2011, **99**, 328–337.
32 G. M. Halpenny, K. R. Gandhi and P. K. Mascharak, *ACS Med. Chem. Lett.*, 2010, **1**, 180–183.
33 M. Madhani, A. K. Patra, T. W. Miller, A. A. Eroy-Reveles, A. J. Hobbs, J. M. Fukuto and P. K. Mascharak, *J. Med. Chem.*, 2006, **49**, 7325–7330.
34 Y. Hitomi, K. Arakawa, T. Funabiki and M. Kodera, *Angew. Chem., Int. Ed.*, 2012, 51.
35 Y. Hitomi, K. Arakawa and M. Kodera, *Chem.–Eur. J.*, 2013, **19**, 14697–14701.
36 D. J. Cooper, M. D. Ravenscroft, D. A. Stotter and J. J. Trotter, *J. Chem. Res., Miniprint*, 1979, 3359.
37 W. R. Scheidt, K. Hatano, G. A. Rupprecht and P. L. Piciulo, *Inorg. Chem.*, 1979, **18**, 292–299.
38 P. L. Piciulo, G. Rupprecht and W. R. Scheidt, *J. Am. Chem. Soc.*, 1974, **96**, 5293–5295.
39 J. V. Garcia, F. Zhang and P. C. Ford, *Philos. Trans. R. Soc. A*, 2013, **317**, 20120129.
40 R. C. M. C. Burla, M. Camalli, B. Carrozzini, G. L. Cascarano, L. D. Caro, C. Giacovazzo, G. Polidori and R. J. Spagna, *Appl. Crystallogr.*, 2005, 381–388.
41 G. M. Sheldrick, *SHELX97: Programs for the Solution and Refinement of Crystal Structures, Univ. of Göttingen, Göttingen, 1997*, Univ. of Göttingen, Göttingen, 1997.
42 M. Montalti, A. Credi, L. Prodi and M. T. Gandolfi, *Handbook of Photochemistry*, CRC Press, Boca Raton, 3rd edn, 2006.